DESIGN AND OPTIMIZATION OF A HORN FOCUSING SYSTEM FOR EFFICIENT PION CAPTURE IN A MUON COLLIDER DEMONSTRATOR

P. Rao*, S. Dasu, C.-H. Nee, R. Alharthy, M. Hedges, C. Vuosalo
University of Wisconsin–Madison, Madison, WI, USA
P.-B. Jurj, R. Kamath, Imperial College London, London, UK
K. Yonehara, D. Stratakis, S. Jindariani, J. Eldred
Fermi National Accelerator Laboratory, Batavia, IL, USA

Abstract

This study investigates magnetic horn focusing as a lower-cost alternative to superconducting solenoids for the Muon Collider Demonstrator. We optimized a single horn for pion capture in the 100 MeV/c to 400 MeV/c range using a Bayesian pipeline with a Tree-structured Parzen Estimator. The optimized structure is benchmarked against IMCC baselines and the solenoid channel using FLUKA 2025.1.1 and GEANT4 (geant4-v11.3.2) simulations, providing a quantitative assessment of the horn/solenoid trade-off.

INTRODUCTION

Muon colliders are a compelling option for future high-energy lepton collisions, but their realization depends on efficient muon production and cooling. The conventional approach to pion capture in the muon-production front end relies on superconducting solenoids, which are technically challenging and costly. Magnetic horns, routinely used in neutrino experiments, offer a cost-effective alternative: they focus charged pions of one sign using a pulsed toroidal magnetic field, requiring no superconducting technology.

This paper reports on the design and Bayesian optimization of a single horn for the Muon Collider Demonstrator [3]. The objective is to maximize π^+/μ^+ with $0.2 \le E \le 0.5$ GeV inside a 4D acceptance ellipse, providing the first step toward a complete double-horn design. We describe the target/horn geometry, simulation framework, results, and the exact physics model used by the optimizer.

HORN DESIGN AND SETUP

Beam and Target

An 8 GeV proton beam with Gaussian transverse profile ($\sigma = 4.71$ mm) strikes a tungsten target (radius 6 mm, length 10 cm, $\rho = 19.3\,\mathrm{g/cm^3}$) centered at $z \approx 26$ cm. Earlier studies used a graphite target; the switch to tungsten improves pion production rate per unit length owing to the higher nuclear interaction cross-section [2].

Horn Geometry

The focusing system, illustrated in Fig. 1, consists of three coaxial regions:

- *Neck* ($z = 20$–45 cm): aluminum tube with $r_0 = 2.0$ cm and a 2 mm wall.

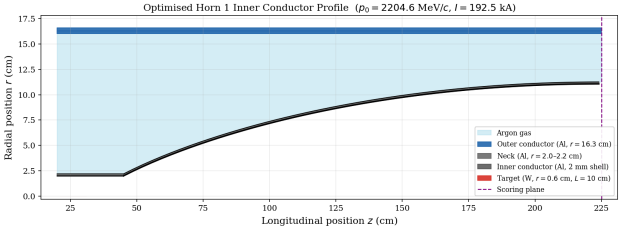

Figure 1: Optimized Horn 1 profile. The inner conductor expands from $r_0 = 2.0$ cm to $r_f = 11.06$ cm; the dashed line marks the scoring plane at $z = 224.0$ cm.

Table 1: Best-Performance Design Parameters

Parameter	Value
Horn length	179.0 cm
Bore radius r_0	2.0 cm
Final inner radius r_f	11.06 cm
Outer conductor radius	16.3 cm
Horn current I	192.5 kA
Twiss (α_x, β_x)	$(-0.24,\ 55.1$ cm)
Twiss (α_y, β_y)	$(-0.25,\ 54.6$ cm)

- *Inner conductor* ($z = 45$–224 cm): 2 mm aluminum shell expanding to $r_f = 11.06$ cm in 50 TRC segments.
- *Outer conductor*: straight aluminum cylinder with $r = 16.3$ cm; argon fills the gap.

From the outside the horn appears as a coaxial cylinder ≈ 2.2 m long and 33 cm in outer diameter with pulsed power feedthroughs at each end. Key optimized parameters are listed in Table 1.

Magnetic Focusing Principle

Current I flows in the $+z$ direction through the inner conductor, producing $B_\phi = \mu_0 I/(2\pi r)$ in the gap. The field focuses π^+ inward and defocuses π^-, making the horn sign-selective. The goal is to redirect large-angle pions so they exit with $p_r \approx 0$; overly strong focusing sends small-radius pions into the conductor wall and is penalized by the optimizer.

SIMULATION RESULTS

Horn results use FLUKA 2025.1.1 [4,5] with 10^5 primary 8 GeV protons; solenoid comparisons use GEANT4 (geant4-v11.3.2). A custom `MGDRAW` routine records particle type, phase-space coordinates, momentum, and arrival time at

* pprao@wisc.edu

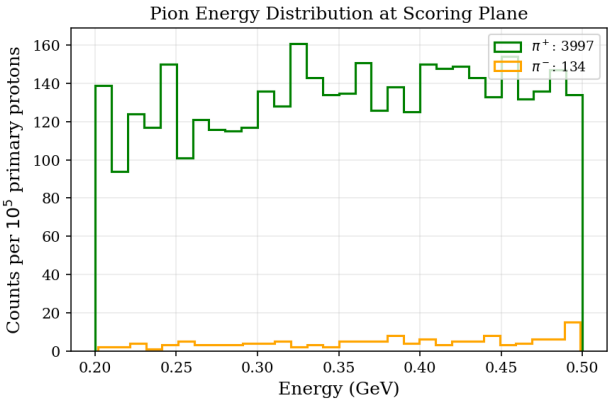

Figure 2: Pion energy distribution at the scoring plane for $0.2 \le E \le 0.5\,\mathrm{GeV}$ and 10^5 primary protons. Green: π^+; orange: π^-.

$z = 224.0\,\mathrm{cm}$. The energy-spectrum, time-structure, and phase-space studies use $0.2 \le E \le 0.5\,\mathrm{GeV}$, the parent-pion band relevant for downstream muon production. The transverse phase-space analysis also applies a $0.2\,\mathrm{cm}\cdot\mathrm{rad}$ 4D acceptance cut, about $2\,\mathrm{mm}\cdot\mathrm{rad}$.

Pion Yield and Energy Spectrum

Figure 2 shows the total-energy distribution of π^+ and π^- in the selected $0.2 \le E \le 0.5\,\mathrm{GeV}$ window at the scoring plane. The π^+ spectrum (green) peaks near $E \sim 0.5\,\mathrm{GeV}$, corresponding to pions whose transverse momentum has been efficiently redirected into the longitudinal direction by the horn field. The π^- yield (orange) is suppressed by the same toroidal field that focuses π^+, demonstrating the sign-selectivity of the horn.

Momentum Distribution

Figure 3 shows the π^+ density in the (p_z, p_r) plane. The dashed lines mark the $0.2 \le E \le 0.5\,\mathrm{GeV}$ objective window. Pions populate a ridge with decreasing p_r as p_z increases, showing the transfer of transverse into longitudinal momentum; the dense region near $p_r \approx 0$ gives the captured signal.

Beam Time Structure

Figure 4 shows selected π^+ in the (arrival time, energy) plane. Relativistic pions traveling $\approx 2.2\,\mathrm{m}$ arrive near $t \approx 7.5\,\mathrm{ns}$. The energy–time correlation reflects the pion velocity spread and sets the required horn-current pulse width.

Transverse Phase Space

Figure 5 shows the x–x' phase space of selected π^+/μ^+ with $0.2 \le E \le 0.5\,\mathrm{GeV}$. The red ellipse marks the $0.2\,\mathrm{cm}\cdot\mathrm{rad}$ 4D acceptance boundary. The sample has RMS emittances $\varepsilon_x = 604\,\mathrm{mm\,mrad}$ and $\varepsilon_y = 478\,\mathrm{mm\,mrad}$, with $\alpha_x = -0.20$ and $\alpha_y = -0.26$; 409 of 4491 particles lie inside the acceptance.

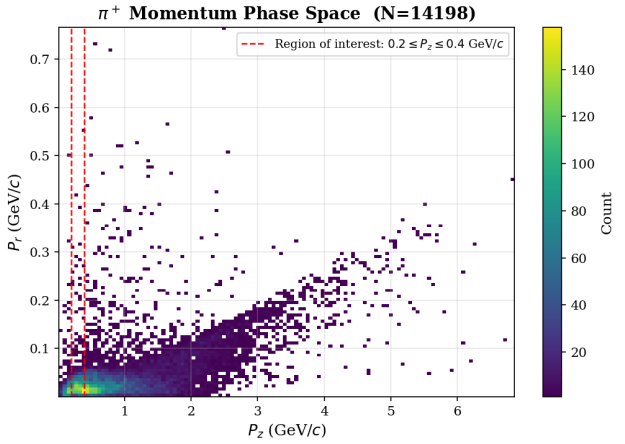

Figure 3: π^+ longitudinal vs. transverse momentum at the scoring plane. Dashed lines mark $0.2 \le E \le 0.5\,\mathrm{GeV}$; colour gives particle density.

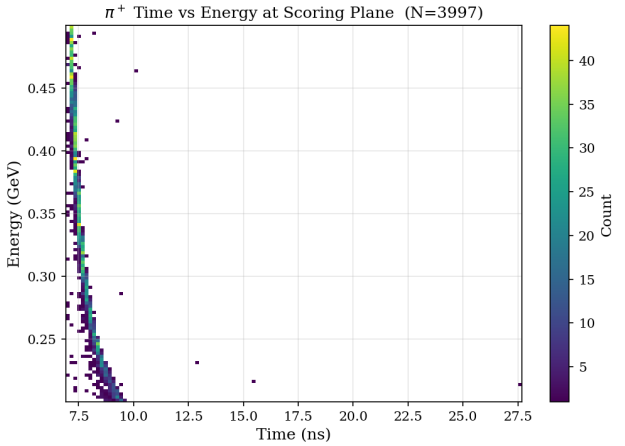

Figure 4: Selected π^+ arrival time vs. energy at the scoring plane for $0.2 \le E \le 0.5\,\mathrm{GeV}$ and 10^5 primary protons.

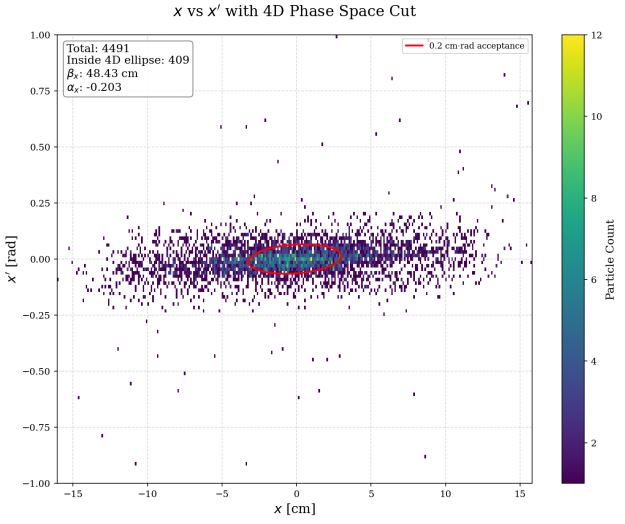

Figure 5: x–x' phase space of selected π^+/μ^+. Colour gives density; the red ellipse is the $0.2\,\mathrm{cm}\cdot\mathrm{rad}$ 4D acceptance.

BAYESIAN OPTIMISATION AND PHYSICS MODEL

Optimisation Framework

The horn geometry is parameterised by design momentum p_0, longitudinal fraction $p_{z,0}/p_0$, and current I. Each trial computes the conductor profile analytically, discretises it into 50 TRC segments, embeds it in the FLUKA input deck, and simulates it. Optuna [6] with the Tree-structured Parzen Estimator (TPE) proposes trials over:

- $p_0 \in [500, 3000]\,\mathrm{MeV}/c$
- $p_{z,0}/p_0 \in [0.90, 0.999]$
- $I \in [50, 200]\,\mathrm{kA}$

Objective Function

The score is

$$\mathscr{S} = n_{4D}\,\exp(-\frac{1}{2}(\alpha_x^2 + \alpha_y^2)), \tag{1}$$

where n_{4D} counts π^+/μ^+ with $0.2 \le E \le 0.5\,\mathrm{GeV}$ inside the $0.2\,\mathrm{cm}\cdot\mathrm{rad}$ 4D acceptance, and $\alpha_{x,y}$ are the Twiss alpha parameters. The penalty suppresses strongly converging or diverging beams.

Physics Model of the Inner Conductor

The inner conductor profile follows from the exact relativistic equations of motion in the toroidal field. Because the magnetic force is perpendicular to velocity, total momentum p_0 is conserved. The focusing constant is

$$k = \frac{\mu_0 q I}{2\pi}\,. \tag{2}$$

The final radius and initial angle are

$$r_f = r_0 \exp\!\left(\frac{p_0 - p_{z,0}}{k}\right), \tag{3}$$

$$\phi_0 = \arcsin\frac{p_{z,0}}{p_0}\,. \tag{4}$$

For Trial 97, $k = 11.54\,\mathrm{MeV/c}$, $r_f = 11.06\,\mathrm{cm}$, $\phi_0 = 82.4°$.

Momentum evolution. The equation of motion $dp_z/dr = k/r$ integrates to:

$$p_z(r) = p_{z,0} + k\ln\!\left(\frac{r}{r_0}\right), \tag{5}$$

$$p_r(r) = \sqrt{p_0^2 - [p_z(r)]^2}\,. \tag{6}$$

Trajectory differential equation.

$$\frac{dz}{dr} = \frac{p_z(r)}{p_r(r)} = \frac{p_{z,0} + k\ln(r/r_0)}{\sqrt{p_0^2 - [p_{z,0} + k\ln(r/r_0)]^2}}\,. \tag{7}$$

The total horn length in r is

$$L = \int_{r_0}^{r_f} \frac{p_{z,0} + k\ln(r/r_0)}{\sqrt{p_0^2 - [p_{z,0} + k\ln(r/r_0)]^2}}\,dr\,. \tag{8}$$

Because this integrand diverges as $r \to r_f$, the angular parameterisation below is used in practice.

Angular parameterisation (ϕ-form). Setting $p_z = p_0\sin\phi$ gives:

$$r(\phi) = r_0\exp\!\left(\frac{p_0\sin\phi - p_{z,0}}{k}\right). \tag{9}$$

This yields the stable slope

$$\frac{dz}{d\phi} = \frac{r_0 p_0}{k}\,\sin\phi\,\exp\!\left(\frac{p_0\sin\phi - p_{z,0}}{k}\right). \tag{10}$$

and horn length

$$L = \int_{\phi_0}^{\pi/2} \frac{r_0 p_0}{k}\,\sin\phi\,\exp\!\left(\frac{p_0\sin\phi - p_{z,0}}{k}\right) d\phi\,, \tag{11}$$

where $\phi = \pi/2$ corresponds to a particle parallel to the z-axis, so $p_r \to 0$ at r_f by construction.

Why the exact formulation is required. The paraxial approximation used in high-energy horn designs such as NuMI [2] treats $p_z \approx p_{z,0}$ and yields a parabolic conductor. For 100–400 MeV/c pions, emission angles reach 15°–20° and $\Delta p_z/p_0 \gtrsim 15\%$, so path-length corrections are significant and the parabolic shape under-focuses the beam. Equations (5)–(11) are therefore used directly for each candidate conductor shape.

CONCLUSION

We have presented a FLUKA-based design and Bayesian optimization of a magnetic horn for pion capture in the Muon Collider Demonstrator. The exact relativistic trajectory model handles large-angle 100–400 MeV/c pions and parameterises the horn with three physics-motivated variables. The best design (Trial 97, $p_0 = 2204.6\,\mathrm{MeV/c}$, $I = 192.5\,\mathrm{kA}$) achieves 285 signal π^+ per 10^4 primary protons in the acceptance window with modest Twiss α values, supporting a double-horn optimization and systematic benchmarking against the IMCC solenoid baseline.

REFERENCES

[1] C. Accettura *et al.*, "Towards a Muon Collider", *Eur. Phys. J. C*, vol. 83, p. 864, 2023. doi:10.1140/epjc/s10052-023-11889-x

[2] S. Kopp, "The NuMI neutrino beam at Fermilab", *AIP Conf. Proc.*, vol. 773, p. 276, 2005. doi:10.1063/1.1949544

[3] F. Ballarini *et al.*, "The FLUKA code: Overview and new developments", *EPJ Nucl. Sci. Technol.*, vol. 10, p. 16, 2024. doi:10.1051/epjn/2024010

[4] G. Battistoni *et al.*, "Overview of the FLUKA code", *Ann. Nucl. Energy*, vol. 82, pp. 10–18, 2015. doi:10.1016/j.anucene.2014.11.007

[5] T. Akiba *et al.*, "Optuna: A Next-generation Hyperparameter Optimization Framework", in *Proc. 25th ACM SIGKDD*, Anchorage, AK, USA, Aug. 2019, pp. 2623–2631. doi:10.48550/arXiv.1907.10902